Bulk Crystallization of Isotactic Polystyrene near Its Melting Point: A Neutron Scattering Study of the Chain Trajectory

Jean-Michel Guenet* and Claude Picot

Centre de Recherches sur les Macromolecules (CNRS), 67083 Strasbourg Cedex, France.
Received March 24, 1982

ABSTRACT: The study of the chain trajectory in isotactic polystyrene (IPS) crystallized near its melting point (temperature of crystallization = 220 °C) has been accomplished through the use of small-angle neutron scattering (SANS). As in previous experiments, no isotopic segregation has been observed after crystallization, so the results reported here are really related to the single-chain behavior. The samples have been characterized by optical microscopy and DSC. The morphology turns out to be quite similar to that of isolated single crystals. The interpretation of the results leads to a sheetlike conformation that arises from adjacent reentry along the 330 plane as in IPS solution-grown single crystals. The validity of the model is discussed in light of alternative trajectories recently proposed for polyethylene.

Introduction

We have recently reported[1-3] small-angle neutron scattering (SANS) experiments carried out on isotactic polystyrene (IPS) intended to determine the chain trajectory in a semicrystallized medium. We have shown the chain conformation to be fairly dependent upon both the crystallization temperature and the matrix molecular weight. For example, concerning melt-crystallized samples we have pointed out the existence of three different models[4,5] (ACA model, central core model, and "garland" model) that are governed by the variation of the aforementioned parameters. We have concluded that the chain trajectory within the crystalline structures is essentially influenced by the chain mobility in the original amorphous melt. Increasing mobility gives rise to more regular adjacent folding.

This statement has been verified in the case of single crystals grown from dilute solutions,[2] where the chain mobility is high. Here, the SANS results reveal the chain to be nearly completely folded along the 330 plane so as to generate a sheetlike conformation.

However, the morphology in both crystallization processes is dissimilar. In the melt-crystallized samples we have studied, the texture is mainly spherulitic, while in solution-grown samples, isolated crystals predominate.

In order to bridge the gap between the two crystallization processes, we have examined systems crystallized at T_c = 220 °C, which happens to be near the melting point of an infinite IPS crystal (T_m = 242 °C).[6] In this way, the crystallization occurs from the melt but produces a morphology quite similar to that of isolated single crystals.

The purpose of this paper is therefore to report SANS experiments on such systems characterized by the classic techniques (microscopy, DSC) and to discuss the results in light of suitable trajectory models.

Experimental Section

Sample Preparation. The deuterated and hydrogenated polystyrenes (respectively IPSD and IPSH) have been synthesized by the usual Natta method.[7] A full description of the preparation, tacticity characterization, and molecular weight and polydispersity determinations is given in ref 8. Presently, four different deuterium-labeled samples of narrow polydispersities have been used (see Table I), with, as to the experiments in the crystalline state, an IPSH matrix of weight average $M_w = 5.6 \times 10^5$ and of polydispersity M_w/M_n = 3.33.

Solid solutions containing approximately 2–3% of IPSD chains in the IPSH matrix have been prepared by dissolving in boiling chlorobenzene and then coprecipitating by dropwise addition into methanol. Transparent disk-shaped samples 1 mm thick have been obtained by molding the as-recovered powder at 250 °C under vacuum and then quenching rapidly to room temperature. The crystallization process has been achieved under vacuum in an oven kept at 220 ± 1 °C for 8 days. Afterward, the as-crystallized samples have been compression-molded at 220 °C so as to reshape them and to minimize the amount of microvoids.

Table I
Experimental Results[a]

$10^{-5}M_w$ (IPSD)	M_w/M_n	$R_{g_{cry}}$ (220 °C)	$R_{g_{am}}$ (220 °C)	$R_{g_{cry}}$(sgsc)
2.5	1.15	133 ± 15	108 ± 4	
3	1.2	152 ± 15	116 ± 4	
5	1.2	206 ± 20	150 ± 10	310 ± 30
7	1.32	263 ± 25	176 ± 10	

[a] $R_{g_{cry}}$(220 °C) = radius of gyration for 220 °C crystallized samples. $R_{g_{am}}$(220 °C) = radius of gyration in an APSH matrix molded at 220 °C. $R_{g_{cry}}$(sgsc) = radius of gyration in solution-grown single crystals (sample previously used in ref 2).

Finally, solid solutions containing the same previous labeled chains but with an atactic matrix instead have been made under the same conditions. They have been molded at 220 °C for 20 min and then quenched rapidly to room temperature so as to freeze in the conformation adopted by the chains at 220 °C. The purpose of preparing such samples is twofold: (1) The measurement of the scattered intensity by amorphous IPS chains in the molten state at 220 °C can be performed since the use of an atactic matrix prevents any crystallization. The comparison between the SANS results obtained from the molten state and from the crystalline state is essential to detect any conformational change. (2) It is of importance to determine the scattering from the melt at precisely 220 °C for we have shown the IPS chain mean dimensions to be temperature dependent in an amorphous surrounding.[9]

Sample Characterization. (a) Optical Microscopy. A reference sample was crystallized under the same conditions as detailed above to characterize the morphology by means of microscopy. This sample consists of a thin layer of IPSH prepared on a glass slide by evaporating a 5% THF solution and then heating the slide to 250 °C so as to clear up all the crystalline structures. The pictures of Figure 1 reveal the morphology to be comparable to that of single crystals grown from dilute solutions.[2] Here, however, the features happen to be far better defined with their highly hexagonal symmetry observed on only rare occasions. Eventually, one may notice the presence of screw dislocations.

(b) Differential Scanning Calorimetry (DSC). DSC experiments have been carried out with a Perkin-Elmer DSC 2 device using approximately 5 mg of material placed in a sealed sample pan. Only one melting peak has been observed, as seen in Figure 2, where a typical thermogram is drawn. An extrapolated melting point of 231 ± 1 °C has been found by performing experiments at different heating rate (Figure 3). From this value and from relations between the lamellar thickness l_c and melting temperature,[10,11] a value of 127 Å has been deduced.

From the melting area a crystallinity of x_c = 37–40% has been measured by calibrating the apparatus with indium (ΔH_{In} = 6.9

0024-9297/83/2216-0205$01.50/0

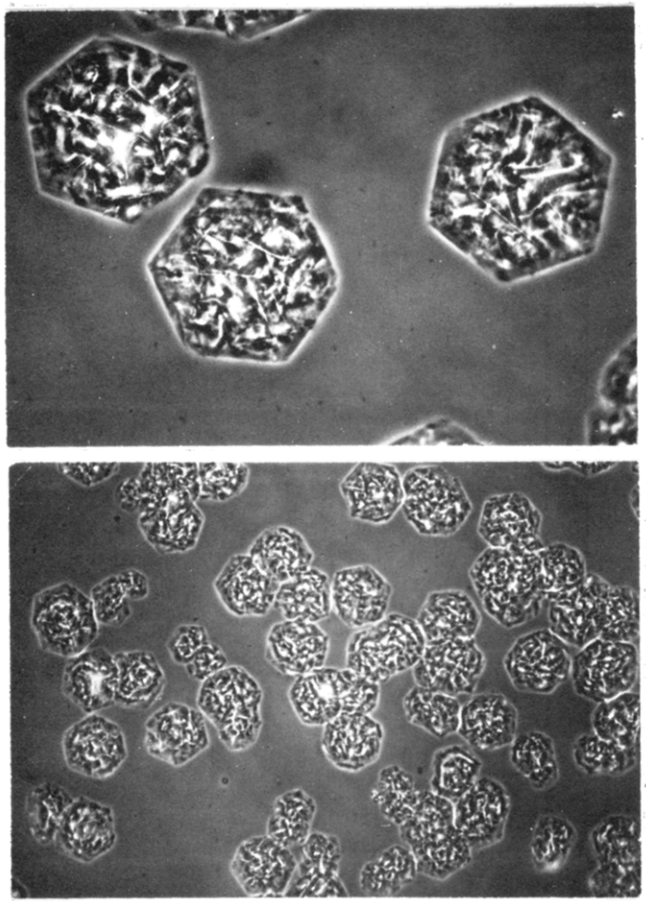

Figure 1. Optical micrographs obtained with Zeiss PM2 microscope: (a) isolated structures—one may notice the highly hexagonal symmetry (size, approximately 10 μm); (b) lower magnification showing some clusters of the crystalline structures.

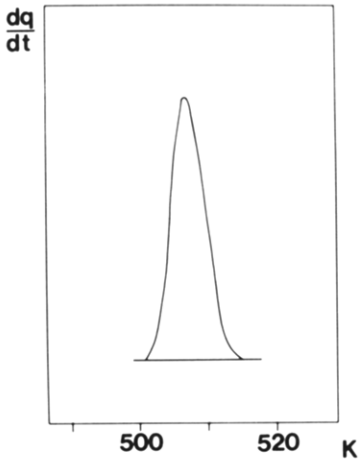

Figure 2. DSC thermogram of 220 °C crystallized IPS; heating rate 10 °C/min.

cal g) and using a value of $\Delta H_{IPS} = 8.6 \times 10^8$ erg/cm^3 [12] for a perfect IPS crystal. As the value of the crystallinity is lower than that measured for single crystals (~70%), one may assume the presence of free amorphous chains not incorporated into the crystals. To check that point, we have attempted to extract them by plunging the samples into THF for 2 months. After that treatment the crystallinity increased up to 56%. Yet free amorphous material may possibly remain within the sample although its amount must be small since the glass transition of the amorphous chains located near 100 °C is absent for this latter case (but is visible for nonextracted samples). It is noteworthy to mention that the SANS measurements have been carried out on nonextracted material. This will be considered further for the interpretation of the data.

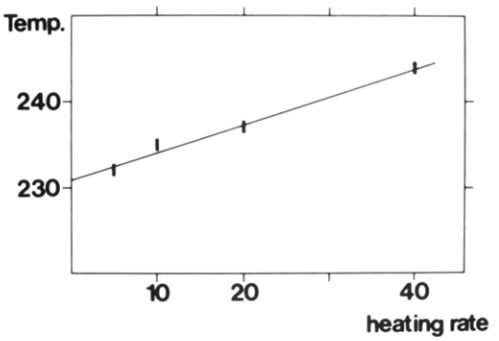

Figure 3. Melting temperature of 220 °C crystallized IPS samples for different heating rates.

Neutron Scattering. The experiments reported in this paper have been performed at the ILL high-flux reactor in Grenoble, France, on D11 and D17 cameras.[13] The scattering vectors $q = (4\pi/\lambda) \sin(\theta/2)$ ranged from $5 \times 10^{-3} \leq q$ (Å^{-1}) $\leq 1.5 \times 10^{-2}$ for D11 and $10^{-2} \leq q \leq 7.5 \times 10^{-2}$ for D17. For both cameras a mechanical monochromator was employed providing a wavelength distribution characterized by a width at half-height $\Delta\lambda/\lambda$ of about 10%.

All the results have been adjusted by using an H-water spectrum for counter normalization, allowing for the junction between data obtained at high q on D11 and low q on D17. A reference sample[9] (IPSD with $M_w = 5 \times 10^5$ in an APSH matrix) has been used for absolute intensity calibration, which allows any eventual isotopic segregation to be spotted and a continuity with the previous experiments to be maintained. Furthermore, as the system exhibits a morphology of single crystals, previous samples made with solution-grown single crystals have been run for comparison in the meantime.

In this paper, the problem of neutron scattering by semicrystalline polymers will not be examined since it has been already discussed in detail elsewhere.[1,2]

Results

Owing to the neutron wavelength (λ ~5–10 Å), two ranges of scattering vectors are usually distinguished when a conformation of radius of gyration R_g is studied:

(1) Guinier Range. In this domain, defined by $qR_g < 1$, the scattered intensity reflects mainly the long-distance correlations and reads

$$I(q) \sim M_w(1 - q^2R_g^2/3) \quad (1)$$

where M_w is the weight-average molecular weight of the labeled chain.

(2) Intermediate Range ($qR_g > 1$). Here, the short-distance correlations predominate, but the effects of crystal diffraction are still far away. The intensity tends to an asymptote expressed as

$$I(q) \sim q^{-n} \quad (2)$$

where n is an exponent depending on the molecular shape. Sometimes, two asymptotes may be observed as in the semidilute systems.[14]

Guinier Range. Results obtained on D11 in the Guinier range are listed in Table I. Once more, it is worthwhile to emphasize that no isotopic segregation occurred during the crystallization process as ascertained by the Zimm plot of intensity in Figure 4. The extrapolated values at $q = 0$, related to the inverse of the molecular weight, are identical for both the amorphous reference sample and the semicrystalline sample.

From the values of mean dimensions in the semicrystalline state, the following variation as function of molecular weight may be deduced:

$$R_g \sim M_w^{0.76\pm0.06} \quad (3)$$

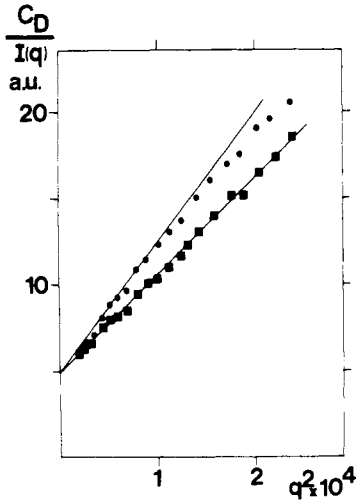

Figure 4. Zimm plot of the intensity in the Guinier range ($C_D/I(q)$ vs. q^2). Black squares stand for M_w(IPSD) = 5×10^5 in APS matrix; T(prep) = 180 °C (reference sample). Black circles stand for 220 °C crystallized sample with M_w(IPSD) = 5×10^5 as well. The intercept at $q = 0$ is the same, showing the absence of isotopic segregation in the semicrystalline sample.

as opposed to the relation obtained with the atactic matrix samples:

$$R_g \sim M_w^{0.5\pm0.02} \tag{4}$$

Finally, one may notice the increase of the radius of gyration after crystallization.

Intermediate Range. An examination of the behavior in the intermediate range has been achieved by means of the D17 device. Results are plotted according to a Kratky representation ($q^2I(q)$ vs. q) in Figure 5, a and b, for respectively a 220 °C crystallized sample with the corresponding amorphous sample and for the 220 °C crystallized sample with a single-crystal sample. From Figure 5a, one discovers the different behavior before and after crystallization. The curves obtained from 220 °C crystallized system and from single crystals (Figure 5b) also exhibit similarities. One observes in both cases a q^{-1} behavior ($q < q^*$) followed by a q^{-2} behavior ($q > q^*$). The only difference lies actually in the position of the crossover vector q^*, which happens to be $q^* = 2.7 \times 10^{-2}$ for the single crystals and $q^* = 1.8 \times 10^{-2}$ for the 220 °C crystallized systems. The values $n = 1$ and $n = 2$ determined from these plots have been checked by using a double-logarithmic scale ($\log I(q)$ vs. $\log q$).

Discussion

Before attempting to interpret the above experimental results, we have to define as precisely as possible the samples we are dealing with.

From the DSC measurements, it turns out that the system is actually a mixture of chains crystallized in one lamella on the one hand and free amorphous chains on the other. The first task consists in evaluating the amount of these uncrystallized chains. Supposedly, the crystallinity z within the lamella ought to be close to that previously measured for solution-grown single crystals for which all the uncrystallized material was removed (≃70%). Through this assumption, it is easy to determine the amount y of crystalline species within the sample according to

$$y = \frac{x_c}{z} \simeq 0.4/0.7 \simeq 0.57 \tag{5}$$

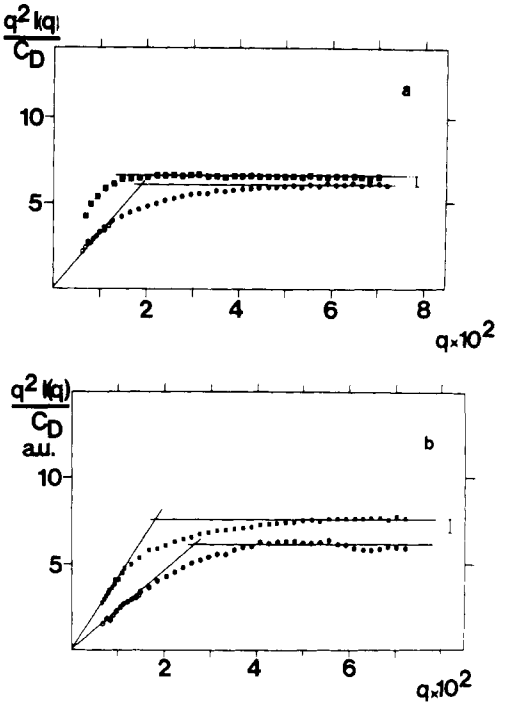

Figure 5. (a) Kratky representation of the reduced intensity in the intermediate range ($q^2I(q)/C_D$ vs. q). Circles stand for the 220 °C crystallized samples, where M_w(IPSD) = 5×10^5 (opened circles stand for the highest angles on D11). Black squares stand for M_w(IPSD) = 5×10^5 in APSH matrix molded at 220 °C. For clarification of the figure the upper curve has been shifted upward by a factor of 1.1. (b) Same representation as Figure 5a. Circles stand for solution-grown single crystals with M_w(IPSD) = 5×10^5. Squares stand for 220 °C crystallized sample with $M_w = 7 \times 10^5$. The upper curve has been shifted upward by a factor of 1.1 to clarify the figure (opened circles and squares stand for highest angle on D11).

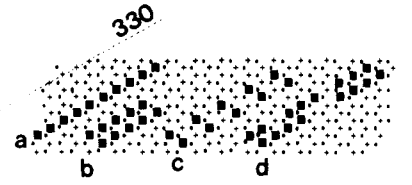

Figure 6. Partial sketch of IPS crystal seen from above. Crosses stand for right-hand helix and circles for left-hand helix or vice versa. Magnified black squares stand for stems occupied by a labeled chain: (a) adjacent reentry along 330; (b) adjacent reentry along 330 with "superfolding"; (c) next adjacent reentry along 330 with "superfolding"; (d) adjacent reentry along 330 by bunching.

where x_c is the overall crystallinity. Consequently, the amount of free amorphous chains is

$$1 - y \simeq 0.43 \tag{6}$$

Incidentally, the crystallinity measured after THF extraction indicates that, by this method, approximately 20% of uncrystallized chains have been extracted ($y = 0.56/0.7 = 0.8$), which confirms the above assumptions.

As a consequence, the intensity scattered by the labeled chains embedded in the 220 °C crystallized samples must be written

$$I(q) = yI_c(q) + (1 - y)I_a(q) \tag{7}$$

with obvious meaning as to the subscripts and with $y = 0.57$.

As it turns out, the SANS results are fairly reminiscent of those obtained from solution-grown single crystals;[2] we shall restrict our interpretation to semicrystalline models

Table II
Experimental and Calculated Values (from Relations 8 and 9) of the Radii of Gyration in Samples Crystallized at 220 °C[a]

$10^{-5}M_w$ (IPSD)	$R_{g_{expt}}$	ν_{expt}	$R_{g_{th}}$	ν_{th}
2.5	133 ± 15	0.76 ± 0.06	118	0.82
3	152 ± 15		138	
5	206 ± 20		212	
7	263 ± 25		286	

[a] Although the theoretical expression relating the radius of gyration to the molecular weight is not actually of the form $R_g \sim M^\nu$ (see relation 9), we have nevertheless calculated a mean exponent ν_{th} for the four considered molecular weights by means of a mean least-squares method. In fact, the difference between the actual variation and the classical $R_g \sim M^\nu$ variation is negligible.

of chain trajectory envisaged in this situation (see Figure 6). Thus the switchboard model or models with chain entering different lamella have to be dismissed for the reasons invoked in ref 2. The data gathered on IPS solution-grown single crystals[2] are quite consistent with the sheetlike model built up from the adjacent folding along the 330 plane (model a in Figure 6). We shall therefore first take into consideration this model for interpreting the above results.

In the Guinier range, we have the following relation as to the radius of gyration:

$$\langle R_g^2 \rangle = y\langle R_c^2 \rangle + (1-y)\langle R_a^2 \rangle \tag{8}$$

in which $\langle R_c^2 \rangle$ is expressed according to[4]

$$\langle R_c^2 \rangle = \langle r_e^2 \rangle + \frac{z^2M^2}{M_r^2}\frac{\langle l^2 \rangle}{12} \tag{9}$$

where $\langle r_e^2 \rangle \simeq l_c^2/12$, z is the crystallinity within the lamella, M and M_r are respectively the molecular weights of the labeled chain and of the elementary rod incorporated in a stem, and $\langle l^2 \rangle$ is the mean-square reentry length, that is, the distance between two adjacent labeled rods belonging to the same chain.

This equation may be computed numerically since all its parameters are known from experiment. As we are considering adjacent reentry along the 330 plane, we deduce l = 12.6 Å. The choice of that plane arises from energetic considerations. The energy required to change the configuration from a left-hand into a right-hand helix or vice versa is very high ($E \simeq 10$ kcal), which promotes chain incorporation along a plane containing stems of same helicity. For IPS only the 330 plane meets this condition, as illustrated in Figure 6.

By inserting relation 9 into 8 and introducing the experimental values of $\langle R_a^2 \rangle$ listed in Table I, one obtained the theoretical values of R_g gathered in Table II. Evidentally, the computed values of R_g from relation 8 are in good agreement with the experimental ones and the exponents of the law $R_g \sim M^\nu$ as well. The data collected in the intermediate range should provide further information as to the validity of the model that is equivalent to a thin sheet, the form factor of which has been analytically derived by Porod:[15]

$$P_s(q) = \frac{2}{qL_c}\left[\frac{\pi'}{ql_c}\left(\int_0^{ql_c}\frac{J_1(x)}{x}\,dx\right) + \frac{1}{qL_c}\left(\frac{\sin(ql_c/2)}{ql_c/2}\right)^2 - \frac{\sin(qL_c)}{(qL_c)^2}\right] \tag{10}$$

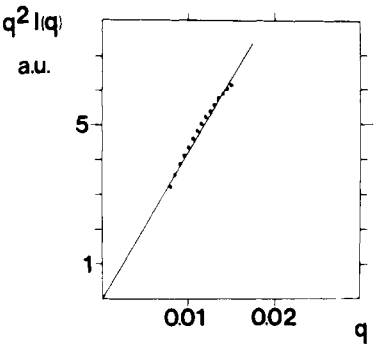

Figure 7. Kratky representation ($q^2I(q)$ vs. q) of the theoretical intensity calculated from relation 13 in the range $ql_c < 1$, $qL_c > 1$. Black circles stand for the theoretical values. Solid straight line shows that relation 13 is nearly linear in this range. Thus, the intensity may be approximated as $I(q) \sim q^{-1}$.

where l_c and L_c are respectively the width and the length of the thin sheet and π' is a complex function tending to π = 3.14... beyond the Guinier regime.

When the mean dimension of the loops between two adjacent rods is small, this relation may be used without any corrections in the scattering vector range we are working with. This particular point has been already discussed in detail in ref 2.

Such a form factor exhibits two types of asymptotic behavior:

$$ql_c \ll 1 \qquad qL_c \gg 1$$
$$\lim P_s(q) = (\pi/qL_c)\exp[-q^2l_c^2/24] \tag{11}$$

where the exponential term is a corrective factor close to unity, and

$$ql_c \gg 1 \qquad qL_c \gg 1$$
$$\lim P_s(q) = 2\pi/q^2L_cl_c \tag{12}$$

By introducing these expressions in relation 7, one may calculate the intensity scattered by the labeled chains in the appropriate q range and particularly determine the exponents or apparent exponents as defined in relation 2. While at larger angles (ql_c and $qL_c \gg 1$) the resulting exponent deduced from relation 7 must be rigorously the same as in relation 12 (n = 2) since in this range the intensity scattered by a Gaussian coil behaves like q^{-2}, in the range $ql_c \ll 1$ and $qL_c \gg 1$, the value of the apparent exponent is not straightforwardly predictable. To estimate its value, one has to consider the following expression as to the scattered intensity:

$$I(q) = M\left[\left(y\frac{\pi}{qL_c}\exp\left(-\frac{q^2l_c^2}{24}\right)\right) + (1-y)\times\left(\frac{2}{q^4R_a^4}[q^2R_a^2 - 1 + \exp(-q^2R_a^2)]\right)\right] \tag{13}$$

where the second term is the well-known Debye form factor for Gaussian chains.

All the parameters of this equation are known, and L_c is derived from

$$L_c^2 = (z^2M^2/M_r^2)l^2$$

Calculations carried out for $M = 5 \times 10^5$ show that the theoretical curve is almost linear in a Kratky representation (Figure 7), which means n_{app} = 1. Despite the nonnegligible amount of amorphous chains, the exponent of expression 11 is virtually unaltered.

Thus experiments performed in the intermediate range are still in good agreement with the sheetlike model as far

as the exponents are concerned.

From the theoretical and experimental intensities, further results may be derived that enable us to test the consistency of the model.

(i) The ratio ρ between the intensities scattered by the 220 °C crystallized samples and the amorphous samples in the q^{-2} behavior domain can be determined as follows: With use of relations 7 and 12, at larger angle $I(q)$ reduces to

$$I(q) \sim M(y(2\pi/q^2 l_c L_c) + (1-y)(2/q^2 R_a^2)) \quad (14)$$

so we are led to

$$\rho_{th} = \frac{y(2\pi/q^2 l_c L_c) + (1-y)(2/q^2 R_a^2)}{2/q^2 R_a^2} \quad (15)$$

which finally yields

$$\rho_{th} = y(\pi R_a^2/L_c l_c) + (1-y) \simeq 0.91 \quad (16)$$

Experimentally, we find from Figure 5a

$$\rho_{exptl} \simeq 1 \quad (17)$$

which is again in good agreement.

(ii) The ratio γ between the intensities scattered by the 220 °C samples and the solution-grown single crystals in the q^{-2} behavior domain can be determined as follows: For the labeled chains in single crystals we have

$$I_{sc}(q) \sim 2\pi M'/q^2 l_c' L_c' \quad (18)$$

Then by application of relation 7, γ reads

$$\gamma_{th} = \frac{I(q)}{I_{sc}(q)} = \frac{M(y(2\pi/q^2 l_c L_c) + (1-y)(2/q^2 R_a^2))}{2\pi M'/q^2 l_c' L_c'} \quad (19)$$

As the incorporation in both cases takes place along the 330 plane, the density of atoms per unit area is the same:

$$M/l_c L_c = M'/l_c' L_c' \quad (20)$$

γ_{th} then reduces to

$$\gamma_{th} = y + (1-y)(l_c L_c/\pi R_a^2) \simeq 1.08 \quad (21)$$

From Figure 5b one obtains experimentally

$$\gamma_{exptl} = 1.12 \quad (22)$$

again in close agreement with the theoretical value.

(iii) The value of the crossover q^* is determined by the intercept of the two asymptotes:

$$y\frac{\pi}{q^* L_c} + (1-y)\left(\frac{2}{q^{*2} R_a^2} - \frac{2}{q^{*4} R_a^4}\right) = y\frac{2\pi}{q^{*2} l_c L_c} + (1-y)\frac{2}{q^{*2} R_a^2} \quad (23)$$

In this scattering vector domain the exponential term in the Debye function is negligible and may be omitted. In addition, we may drop the term containing q^{*4} in first approximation, which leads eventually to

$$q^* = 2/l_c \quad (24)$$

From SANS results $q^* = 1.8 \times 10^{-2}$, leading to $l_c = 111$ Å, a value in good agreement with that derived from DSC.

Hitherto, all the results gained from SANS experiments on 220 °C crystallized samples are fairly well consistent with a chain trajectory arising from adjacent folding along the 330 plane. It is actually not surprising since the crystalline species growing at such a crystallization temperature exhibit a morphology similar to that of single crystals, for which a comparable model has been already put forward.[2] Nevertheless, crystallizing from the melt leads to a polymer concentration in the vicinity of the crystalline growth front far higher than in dilute solutions. It is therefore of importance to discover whether the sheetlike model uniquely explains the SANS data. With this aim, we shall regard alternative models (drawn in Figure 6) and see whether they could account for our results as well.

(i) Adjacent Reentry with "Superfolding". The neologism "superfolding" has been introduced by Sadler and Keller[16] to describe a model accounting for their experimental results on polyethylene. For the case we are interested in, we have slightly modified the model in that the chain, instead of folding backward on an adjacent plane, actually folds back on a plane of same helicity (model b in Figure 6). Should such a model represent the chain trajectory in the crystals, the measured values of the radii of gyration would be smaller by a factor of approximately 2. Therefore it may be discounted.

(ii) Next Adjacent Reentry with "Superfolding" (Model c). The behavior and value of the radius of gyration for this model are virtually the same as the sheetlike model. However, recent calculations performed by Spells and Sadler[17] on the form factor have shown that the intensity scattered in the intermediate range exhibits a noticeable decrease in a Kratky representation (that is, $I(q) \sim q^{-n}$ with $n > 2$), which does not meet our results either.

(iii) Adjacent Reentry in Bunches (Model d). This model has been proposed by the same authors[17,18] as above for interpreting SANS experiments on polyethylene single crystals grown at high undercooling. Here, adjacent reentry occurs by bunching instead of being regular. Such a model may account for the experimental values of the mean dimensions but suffers from an intermediate-domain intensity characterized as previously by an exponent $n > 2$.

Eventually, from all these considerations, nothing but the sheetlike model fits satisfactorily the SANS data. Obviously some deviations may arise due to screw dislocations or crystalline lattice defects. However, this model provides a close picture of the actual features.

Accordingly, the statement on the chain mobility seems to be confirmed. As a matter of fact, in both crystallization processes involved in the formation of single crystals, the chain mobility is high if we refer, as in previous papers[1-3] to the comparison between the time τ_p needed by the crystalline growth front to envelop the dimension of a chain ($\tau_p \simeq R_g/G$) and the long relaxation time τ_m of the chain in the original amorphous medium (in both cases $\tau_m \ll \tau_p$).

Finally, a further conclusion may be drawn as to the sample morphology. Should the mobility be high, the sheetlike model is highly probable, which certainly promotes the formation of single crystals. Seemingly, this effect has been already observed by Keith, Vadimsky, and Padden[19] on a mixture of 10% IPS dispersed in a very low molecular weight APS surrounding. Despite an undercooling ΔT of about 50 °C (T_c = 190 °C) they have been able to grow regularly hexagonal-shaped single crystals.

Conclusion

In this paper, we have reported SANS experiments performed on samples crystallized near the IPS perfect-crystal melting point (T_c = 220 °C) that exhibit a single-crystal morphology. The interpretation of the experimental data leads to the adoption of a sheetlike model for the chain trajectory due to adjacent folding along the 330 plane. The model is similar to that envisaged for solution-grown single-crystal samples.[2]

We have now studied the IPS chain conformation in a wide range of crystallization temperatures.[1-3] So far all the results and interpretations are fairly consistent and demonstrate the existence of several molecular shapes, the presence of which is mainly controlled by the chain mobility in the original amorphous melt or solution.

Acknowledgment. We thank Dr. B. Lotz for the optical microscopy work, G. Pouyet for technical assistance on DSC, and Dr. A. Hässlin for technical assistance in Grenoble.

Registry No. IPS, 25086-18-4; neutron, 12586-31-1.

References and Notes

(1) Guenet, J. M.; Picot, C. *Polymer* **1979**, *20*, 1483.
(2) Guenet, J. M. *Macromolecules* **1980**, *13*, 387.
(3) Guenet, J. M. *Polymer* **1981**, *22*, 313.
(4) Guenet, J. M.; Picot, C. *Polymer* **1979**, *20*, 1473.
(5) Guenet, J. M. *Polymer* **1980**, *21*, 1385.
(6) Lemstra, P. J.; Kooistra, T.; Challa, G. *J. Polym. Sci., Polym. Phys. Ed.* **1972**, *10*, 823.
(7) Natta, G. *J. Polym. Sci.* **1955**, *16*, 143.
(8) Guenet, J. M.; Gallot, Z.; Picot, C.; Benoit, H. *J. Appl. Polym. Sci.* **1977**, *21*, 2181.
(9) Guenet, J. M.; Picot, C.; Benoit, H. *Macromolecules* **1979**, *12*, 868.
(10) Overbergh, N.; Berghmans, H.; Reynaers, M. *J. Polym. Sci., Polym. Phys. Ed.* **1976**, *14*, 1177.
(11) Lauritzen, J. I., Jr.; Hoffman, J. D. *J. Res. Natl. Bur. Stand., Sect. A* **1960**, *65A*, 73.
(12) Dedeurwaeder, R.; Oth, J. F. M. *J. Chem. Phys. Phys.-Chim. Biol.* **1959**, *56*, 940.
(13) Ibel, K. *J. Appl. Crystallogr.* **1976**, *9*, 296.
(14) Farnoux, B.; Daoud, M.; Decker, D.; Jannink, G.; Ober, R. *J. Phys. Lett. (Orsay, Fr.)* **1975**, *36*, 35.
(15) Porod, G. *Kolloid Z.* **1951**, *124*, 83.
(16) Sadler, D. M.; Keller, A. *Macromolecules* **1977**, *10*, 1128.
(17) Spells, S. J.; Sadler, D. M., private communication.
(18) Spells, S. J.; Sadler, D. M.; Keller, A. *Polymer* **1980**, *21*, 1121.
(19) Keith, H. D.; Vadimsky, R. G.; Padden, F. J., Jr. *J. Polym. Sci., Polym. Phys. Ed.* **1970**, *8*, 1687.

Photoresponsive Polymers. 5.[1] Reversible Solubility Change of Polystyrene Having Azobenzene Pendant Groups

Masahiro Irie* and Hisami Tanaka

The Institute of Scientific and Industrial Research, Osaka University, Suita, Osaka 565, Japan. *Received April 19, 1982*

ABSTRACT: The solubility in cyclohexane of polystyrene with a small amount of azobenzene pendant groups (~5 mol % of monomer units) was found to change upon irradiation with light of specific wavelength: ultraviolet light ($410 > \lambda > 350$ nm) caused precipitation of the polymer, while visible light ($\lambda > 470$ nm) resolubilized it. The change of solubility was induced by the photoisomerization of the azobenzene chromophores from the trans to the cis form. Molecular weight distribution measurements of the precipitate and the soluble polymer revealed that the molecular weight of the precipitate ($M_w = 5.4 \times 10^4$, $M_w/M_n = 1.22$) was twice that of the soluble polymer. The dynamics of the precipitation was also studied by a laser photolysis measurement combined with a light scattering detection method.

Introduction

When photoisomerizable chromophores are incorporated into the backbone of polymer chains or into the pendant groups, photoisomerization of the chromophores may affect the physical properties of the polymers and the polymer solutions, especially if isomerization involves appreciable change of a polarity[2] or a geometrical structure. We have recently reported that polymers with spirobenzopyran pendant groups or azobenzene chromophores in the polymer backbone are capable of transforming light energy into reversible alterations of solution viscosity, conductivity, and pH.[1,3-5] Changes of dipole moments of pendant spirobenzopyran groups upon photoirradiation altered the balance of intrachain interaction, resulting in the expansion/contraction of the polymer chains. Geometrical structural changes of the azobenzene residues incorporated in the polymer backbone also caused a conformational change of the polymer chain, affecting solution viscosity, conductivity, and pH. Flash photolysis measurement combined with a light scattering detection method has revealed the relaxation process of unfolding of the above polymer chains.[6]

In this article, we report a reversible solubility change of polystyrene in cyclohexane. Polystyrene with a small amount of azobenzene pendant groups became insoluble in cyclohexane upon irradiation with ultraviolet light, while low molecular weight azobenzene itself did not show any solubility change on photoirradiation. On visible light irradiation, the polymer again became soluble. The dynamics of formation of the precipitation was also studied by a laser photolysis measurement combined with a light scattering detection method.

Experimental Section

Azobenzene chromophores were incorporated into the pendant groups of polystyrene by copolymerization of styrene with 4-(methacryloylamino)azobenzene. Copolymers obtained with a conversion of less than 10% were used for the experiments. 4-(Methacryloylamino)azobenzene was synthesized by the reaction of 4-aminoazobenzene with methacryloyl chloride.[7] The melting point was 150 °C. The azobenzene content of the copolymers was determined by elemental analysis.

Irradiation was carried out with a 1-kW high-pressure mercury lamp and the wavelength was selected with the aid of Toshiba cutoff filters. The laser light scattering measurement apparatus is similar to that described before.[6] The second harmonics of a ruby laser (347 nm) were used as exciting light. An Ar ion laser of 3 W (Spectra-Physics Model 165-07) was used for a scattering light source.

Absorption spectra of the polymer were measured with a Cary 118 spectrophotometer. Polymer precipitation upon irradiation was detected by the decrease of transmittance at 650 nm with a spectrophotometer (Shimadzu UV-200 S). The temperature of the cell was controlled with a temperature-controlled circulating bath (Neslab LT-50). The sample temperature was monitored by a digital thermometer (Doric 410 A), controlled to within ±0.5 °C.

Molecular weight distributions of the polymers were measured by gel permeation chromatography (GPC) with a Toyo Soda H 801 high-speed liquid chromatograph. Molecular weights of the polystyrene with a small amount of azobenzene pendant groups

0024-9297/83/2216-0210$01.50/0